Homozygous *YME1L1* Mutation Causes Mitochondriopathy with Optic Atrophy and Mitochondrial Network Fragmentation

Bianca Hartmann,[1-3§] Timothy Wai,[4§#] Hao Hu,[5,6+] Thomas MacVicar [4], Luciana Musante,[5] Björn Fischer-Zirnsak,[5,7] Werner Stenzel,[8] Ralph Gräf,[9] Lambert van den Heuvel,[10] Hans-Hilger Ropers,[5] Thomas F. Wienker,[5] Christoph Hübner,[2] Thomas Langer,[4] Angela M. Kaindl[1-3]*

[1]Institute of Cell Biology and Neurobiology, Charité University Medicine Berlin, Germany.

[2]Department of Pediatric Neurology, Charité University Medicine Berlin, Germany.

[3]Sozialpädiatrisches Zentrum (SPZ), Center for Chronically Sick Children, Charité University Medicine Berlin, Germany.

[4]Cologne Excellence Cluster on Cellular Stress Responses in Aging-Associated Diseases (CECAD), Institute for Genetics, University of Cologne, Germany.

[5]Max Planck Institute for Molecular Genetics, Berlin, Germany.

[6]Guangzhou Women and Children's Medical Center, Guangzhou, China

[7]Institut of Medical Genetics and Human Genetics, Charité University Medicine Berlin, Germany

[8]Institute of Neuropathology, Charité University Medicine Berlin, Germany.

[9]Department of Cell Biology, Institute for Biochemistry and Biology, University of Potsdam, Germany.

[10]Nijmegen Center for Mitochondrial Disorders at the Department of Pediatrics, Radboud University Medical Center, Nijmegen, the Netherlands.

[#]present address: Institut Necker Enfants Malades, INSERM U1151, CNRS UMR 8253, University Paris Descartes, Paris, France.

[+]present address: Guangzhou Women and Children's Medical Center, Guangzhou 510623, China.

[§]Equal contribution

*Correspondence to: Dr. Angela M. Kaindl, Institute of Cell and Neurobiology, Charité - Universitätsmedizin Berlin, Charitéplatz 1, 10117 Berlin, Germany. Tel/Fax: +49 (0)30 450 566301/7566301. Email: angela.kaindl@charite.de.

Abstract

Mitochondriopathies often present clinically as multisystemic disorders of primarily high-energy consuming organs. Assembly, turnover, and surveillance of mitochondrial proteins are essential for mitochondrial function and a key task of AAA family members of metalloproteases. We identified a homozygous mutation in the nuclear encoded mitochondrial escape 1-like 1 gene *YME1L1*, member of the AAA protease family, as a cause of a novel mitochondriopathy in a consanguineous pedigree of Saudi Arabian descent. The homozygous missense mutation, located in a highly conserved region in the mitochondrial pre-sequence, inhibits cleavage of YME1L1 by the mitochondrial processing peptidase, which culminates in the rapid degradation of YME1L1 precursor protein. Impaired YME1L1 function causes a proliferation defect and mitochondrial network fragmentation due to abnormal processing of OPA1. Our results identify mutations in *YME1L1* as a cause of a mitochondriopathy with optic nerve atrophy highlighting the importance of YME1L1 for mitochondrial functionality in humans.

Running head: *YME1L1* mitochondriopathy

Keywords: YME1L1, mitochondriopathy, intellectual disability, optic atrophy, OPA1, mitochondrial fragmentation

Introduction

Mitochondriopathies often present as multisystemic diseases and can be caused by mutations in nuclear or mitochondrial DNA-encoded genes.[1] Here, we report a novel form of mitochondriopathy with infantile-onset developmental delay, muscle weakness, ataxia, and optic nerve atrophy caused by a homozygous mutation in the yeast mitochondrial escape 1-like 1 gene *YME1L1*.

YME1L1 was first identified in yeast, in a screen for gene products that elevate the rate of mitochondrial DNA migration to the nucleus.[2, 3] The lack of yme1 impairs respiratory growth of yeast highlighting its important function in mitochondrial maintenance.[4, 5] YME1L1, a member of the AAA family of ATPases (ATPases associated with a variety of cell activities), is a nuclear genome-encoded ATP-dependent metalloprotease embedded in the inner mitochondrial membrane (IM), with its protease domain facing the intermembrane space (IMS) (also termed *i*-AAA protease).[6-8] Its import into mitochondria is accompanied by proteolytic processing via the mitochondrial processing peptidase (MPP), which cleaves off the mitochondrial targeting sequence (MTS).[9] The mature protein assembles into a homo-oligomeric complex within the IM.[6, 10] YME1L1 degrades both IMS and IM proteins such as lipid transfer proteins,[11] components of protein translocases of the IM,[12, 13] and the dynamin-like GTPase optic atrophy 1 (OPA1).[14, 13, 15]

The *OPA1* gene (MIM*605290), mutated in dominant optic atrophy[16], encodes a mediator of mitochondrial fusion that also orchestrates mitochondrial cristae morphogenesis.[17-19] OPA1 is processed by two peptidases in the IM, YME1L1 and OMA1 (overlapping with the m-AAA protease 1 homolog), which thereby balance fusion and fission of mitochondria.[20] Long OPA1 forms (L-OPA1) carry out mitochondrial fusion, while short forms (S-OPA1) are dispensable for fusion but contribute to mitochondrial fission when accumulated.[14, 21-24] Loss of YME1L1

accelerates OMA1-dependent L-OPA1 cleavage, resulting in S-OPA1 accumulation, increased mitochondrial fission, and mitochondrial network fragmentation.[14, 25] Despite previous attempts to link YME1L1 to human disease[26], its physiological role in humans remains to be elucidated.

Results and Discussion

Homozygous *YME1L1* missense mutation causes mitochondriopathy

We report for the first time that patients with a homozygous mutation in the *YME1L1* gene develop an infantile-onset mitochondriopathy. Four affected children of healthy, consanguineous parents of Saudi Arabian descent were born at term without complications and with normal anthroprometric data (**Figure 1A**). Medical history gave no indication for perinatal brain damage as a cause for the reported patient phenotypes. All four patients presented with intellectual disability, motor developmental delay, expressive speech delay, optic nerve atrophy associated with visual impairment, hearing impairment, but no facial dysmorphism (**Figure 1B**, **Table 1**). Inconsistent features were microcephaly (II.9, II.11) or macrocephaly (II.5), ataxia (II.5, II.8, II.9), hyperkinesia (II.9), and athetotic and stereotypic movements (II.11). Cranial MRI revealed leukoencephalopathy in all patients and signs of brain atrophy in patients II.9 and II.11 (**Figure 1C**). Lactate levels and lactate/pyruvate ratios were elevated in blood and/or cerebrospinal fluid (CSF) of three patients as indicators of a mitochondriopathy, while alanine levels were normal in blood and cerebrospinal fluid samples. Analysis of a muscle biopsy specimen from patient II.5 revealed mitochondria with altered cristae morphology (so-called 'parking lots') and paracristalline inclusions as well as a neurogenic pattern with grouped fibers indicating denervation, but no conspicuous ragged red fibers in the Gomori trichrome staining (**Figure 1D**). Results of chromosome analysis, mitochondrial DNA sequencing and genetic testing for fragile X syndrome, Nijmegen breakage syndrome, and ataxia teleangiectasia were normal. Similarly, biochemical analyses gave no indication for adrenoleukodystrophy, GM1/GM2 gangliosidoses, Sandhoff disease, Tay-Sachs disease, Gaucher disease, Fabry disease, Krabbe disease, Mucopolysaccharidosis type IVB, neuronal ceroid-lipofuscinoses 1and 2, and congenital disorder of glycosylation (CDG) syndrome (data not shown).

To identify the genetic basis of the disease, we performed whole-exome sequencing (WES) followed by Sanger sequencing and bioinformatic analysis. We thereby identified a homozygous missense mutation in in a highly conserved region of the *YME1L1* gene in the affected children (c.616C>T, NM_014263; chr10:27425300; GRCh 38.5, raw data available: sequence reads archive (SDA) accession no. SRP073309) that segregates with the phenotype in the index family. We did not detect mutations in other genes linked previously to neurologic diseases.[27-29]. The *YME1L1* gene mutation c.616C>T causes the exchange of highly conserved hydrophilic arginine to hydrophobic tryptophan (p. R149W, NP_055078) within the N-terminal MTS (**Figure 1E-G**). YME1L1^{R149W} was below detection levels or profoundly reduced in patient whole cell lysates and in mitochondrial enriched fractions of patient fibroblasts, while mRNA levels remain unaltered (**Figure 1H, I, Figure 1H–Source data 1, Figure 1I–figure supplement 1**). These results identify a disease-causing mutation in arginine 149 of YME1L1, which impairs protein accumulation.

YME1L1^{R149W} abrogates maturation of YME1L1 upon import into mitochondria

The affected amino acid residue arginine 149 is present within a predicted mitochondrial targeting sequence of YME1L1 and may affect targeting of the mutant protein to mitochondria. We therefore transiently expressed YME1L1 and YME1L1^{R149W} in *YME1L1*$^{-/-}$ HeLa cells generated by CRISPR/Cas9-mediated genome editing (**Figure 2A**). Both YME1L1 and YME1L1^{R149W} co-localized with the mitochondrial marker protein ATPase subunit ß, demonstrating mitochondrial targeting of the mutant protein. Consistently, inhibition of the proteasome did not stabilize mutant YME1L1 (**Figure 2B**), suggesting that reduced levels of YME1L1^{R149W} are not caused by proteasomal degradation of non-imported YME1L1 precursor proteins. We therefore excluded a degradation of mutant YME1L1^{R149W} via the proteasome.

Nuclear-encoded YME1L1 requires cleavage of the MTS from premature YME1L1 (~80 kDa) upon import into mitochondria to give rise to the mature protein (~63 kDa), which is able to assemble into a homooligomeric proteolytic complex in the IM.[30, 31, 10] MTS cleavage of YME1L1 precursor is bioinformatically predicted to be mediated by MPP (NM_014263; Mitoprot)[32]. Since the identified human mutation affects an arginine and such residues are known to function as MPP recognition and cleavage sites[33], we asked whether arginine 149 is part of the MPP cleavage site in YME1L1. We mutated various arginine residues in the N-terminal region of YME1L1 and analyzed maturation of corresponding YME1L1 variants synthesized in a cell-free expression system using recombinant MPP (**Figure 2C**). YME1L1 was converted by MPP in its mature form (**Figure 2C**). Mutation of arginine at position 149 abrogated MPP-mediated processing of YME1L1, suggesting that amino acid 151 forms the N-terminal amino acid of mature YME1L1. Replacement of arginine 149 by tryptophan similarly abolished maturation of YME1L1 by MPP *in vitro* (**Figure 2D**).

YME1L1^{R149W} undergoes rapid proteolysis

Grossly reduced YME1L1 protein levels coinciding with unaltered mRNA levels indicate a post-transcriptional mechanism responsible for the reduction of YME1L1^{R149W}. Stabilization of the precursor form of YME1L1 by abolishing the MPP recognition site may allow another peptidase to cleave YME1L1. To identify the latter mechanism, we screened candidate mitochondrial proteases for their effect on YME1L1 and YME1L1^{R149W} stably expressed in HEK293T cells, but could not detect a difference in YME1L1/YME1L1^{R149W} level upon depletion of individual proteases (data not shown). However, by preventing the proteolytic activity of YME1L1 upon ectopic expression of the dominant-negative YME1L1^{E381Q}, harboring a point mutation in the ATPase domain, we were able to stabilize not only the known YME1L1 substrate PRELID1[11] but

149 also observed accumulation of both the precursor and mature forms of YME1L1 (**Figure 3A**).
150 The mature form of YME1L1 remained stable in cells harboring YME1L1^{E381Q} upon further
151 incubation in the presence of cycloheximide, while ectopic expression of the wild type variant
152 resulted in significantly lower levels of YME1L1 and reduced stability (**Figure 3A).** These
153 observations point to an auto-catalytic degradation of YME1L1^{R149W}. We therefore combined the
154 dominant negative mutation E381Q with the pathogenic mutation R149W in YME1L1 in cis and
155 examined the stability of this variant (**Figure 3A**). We observed an accumulation of mature
156 YME1L1$^{R149W/E381Q}$ upon ectopic expression in HEK293T cells (**Figure 3A**). Both mature
157 YME1L1$^{R149W/E381Q}$ and larger forms with a similar size to the precursor form of YME1L1
158 accumulated in these cells. Stabilization of the precursor form of YME1L1 in these cells may
159 allow another peptidase to cleave YME1L1 resulting in the accumulation of slightly smaller
160 forms of YME1L1. These results suggest that YME1L1 mediates degradation of mutant
161 YME1L1^{R149W}, which accumulates in the precursor form due to the mutation of the MPP
162 cleavage site and thus is likely recognized as a misfolded protein in the IM. As the mutant
163 YME1L1 variants were expressed in wild type HEK293T cells, we cannot distinguish whether
164 degradation of YME1L1^{R149W} occurs intramolecularly and/or by endogenous YME1L1 under
165 these experimental conditions. However, the lack of wild-type YME1L1 in patient cells with
166 homozygous *YME1L1* mutations together with our ectopic expression studies argue for auto-
167 catalytic degradation of YME1L1^{R149W}.
168
169 **Impaired proteolysis by YME1L1^{R149W}**
170 To confirm a functional impairment of YME1L1^{R149W}, we analyzed the effect of YME1L1^{R149W}
171 on two substrate proteins, the protein of relevant evolutionary and lymphoid interest (PRELID1)
172 and OPA1, in patient-derived skin fibroblasts. PRELID1, a lipid transfer protein for phosphatidic

173 acid in the IMS, is constitutively degraded by YME1L1.[11] PRELID1 accumulated in primary
174 human fibroblasts (HAF) of patient II.5 when compared to controls (**Figure 3B**), consistent with
175 the low levels of YME1L1^{R149W} present in mitochondria (**Figure 1I**, **Figure 1I–figure**
176 **supplement 1**). Deletion of murine *Yme1l1* leads to accelerated processing of L-OPA1 by
177 OMA1[14, 34] and drives mitochondrial fragmentation *in vitro*[35] and *in vivo*.[36, 25] We similarly
178 identified an altered cleavage pattern of OPA1 in patient cells, albeit more modestly than in
179 knockout mouse cells (**Figure 3C**).
180 This suggests that YME1L1^{R149W} retains proteolytic activity. As proteolysis by YME1L1 depends
181 on its oligomerization, we examined in further experiments the assembly of YME1L1^{R149W}
182 expressed in HEK293 cells by sucrose gradient centrifugation (**Figure 3D**). To allow detection of
183 YME1L1^{R149W} precursor forms and impair its degradation, we also examined the assembly of
184 YME1L1$^{R149W/E381Q}$ expressed in HEK293 cells. Similar to YME1L1, the mutant variants of
185 YME1L1 were recovered in protein complexes of ~2 MDa (**Figure 3D**). Notably, we also
186 observed assembly of the precursor form of YME1L1$^{R149W/E381Q}$, demonstrating that the disease-
187 causing mutation R149W does not impair the formation of the *i*-AAA protease complex. Thus,
188 assembled YME1L1^{R149W} precursor forms may explain the residual activity of YME1L1 in
189 patient fibroblasts (**Figure 3E**). Alternatively, and not mutually exclusive, low levels of mature
190 YME1L1^{R149W} may maintain residual proteolytic activity in the patient system.
191 Together, we conclude that YME1L1^{R149W} is a hypomorphic allele that retains partial YME1L1
192 activity, which reconciles the embryonic lethality[25] of *Yme1l1* knockout mice with the milder
193 phenotype in our patients with a homozygous *YME1L1* missense mutation.
194
195 **YME1L1^{R149W} causes mitochondrial fragmentation**

Given the role of unbalanced mitochondrial dynamics in neurodegenerative diseases[37] and the observed, impaired OPA1 processing, we focused our attention on mitochondrial morphology in patient fibroblasts. We detected an increase in shortened and fragmented mitochondrial networks in HAF of patient II.5 relative to a control (**Figure 4A, B, Videos 1-4, Figure 4B–Source data 1**), consistent with the more severe fragmentation phenotype in *Yme1l1* KO mouse fibroblasts[14]. We therefore transiently expressed human YME1L1^{R149W} and YME1L1 in murine adult cardiac *Yme1l1*$^{-/-}$ fibroblasts[25] and observed that human YME1L1 but not YME1L1^{R149W} was able to complement mitochondrial fragmentation. Of note, the human mutant variant was still able to partially tubulate mitochondria (**Figure 4C, D, Figure 4D–Source data 1**), consistent with the notion that YME1L1^{R149W} retains residual function.

YME1L1^{R149W} impairs cell proliferation

To further address the pathophysiological mechanism underlying the neurological phenotype in humans, we analyzed proliferation and apoptosis of HAF. Proliferation of patient II.5 fibroblasts was significantly reduced compared to those of healthy controls, while the level of induced apoptotic cell death remained unaffected (**Figure 5A-C, Figure 5A–Source data 1, Figure 5B–Source data 1**, **Figure 5C–Source data 1**). Analysis of the respiratory chain in patient fibroblasts revealed the specific enzymatic activities to be within the normal physiological range and subunit levels to be unaltered (**Figure 5D, E**), consistent with the observation in Yme1l1–depleted hearts.[25] However, the reduced steady state levels of various mitochondrial compartment markers in patient cells indicate a general reduction of mitochondrial mass in YME1L1^{R149W} cells (**Figure 5E, Figure 5F**).

Here we report a new form of infantile-onset mitochondriopathy caused by a homozygous mutation in the *YME1L1* gene. Patients suffer from severe intellectual disability, muscular impairments, and optic nerve atrophy. In contrast to complete gene deletion in the mouse,[25] the homozygous c.616C<T missense mutation is compatible with life, likely owing to residual function of YME1L1^{R149W}. We demonstrate that the missense mutation affects the MPP processing site and impairs YME1L1 maturation, leading to its rapid degradation. We further show that the YME1L1^{R149W} leads to a proliferation defect, abnormal OPA1 processing and mitochondrial fragmentation. Since fusion and fission of mitochondria are essential to preserve cellular functions, it is conceivable that defects in these processes, contribute to the patient phenotype in a cell-type specific manner. With our findings we reveal an important role of YME1L1 for the maintenance of mitochondrial morphology in humans and link a loss of YME1L1 function to disease. YME1L1 thereby joins other members of the AAA family of ATPases that have already been linked to neurologic disease, such as spastin (*SPG4*, MIM*6042779 and paraplegin (*SPG7*, MIM*602783) gene, and in the gene encoding the YME1L1 substrate optic atrophy 1 (*OPA1*, MIM*605290).[27, 28, 38, 29] Future studies on further patients are required to determine the full phenotype spectrum associated with *YME1L1* gene mutations.

Material and Methods

Subjects. Informed consent was obtained from the parents of the patients for the molecular genetic analysis, the publication of clinical data, photos, magnetic resonance images (MRI), and studies on fibroblasts. The human study was approved by the local ethics committee of the Charité (approval no. EA1/212/08).

Genetic analyses.

Homozygosity linkage intervals (chr10:24,333,063-49,978,774, LOD=2.533) with LOD>2 and length >1 Mb were identified using the Affymetrix SNP array 6.0. For whole exome sequencing, 1 µg genomic DNA extracted from peripheral blood was enriched by Agilent SureSelect Human All Exon enrichment kit version 3 and deep-sequenced by Illumina Hiseq2000 sequencer in a 101 bp single-end mode. The output sequences amounted to 12 Gb and >94% of the exon-coding regions were covered by at least 20 folds. The data analysis pipeline considered linkage interval, pathogenicity of variants, allele frequency in polymorphism databases (1000Genome, ESP, and an in-house database including 868 individual exomes of Middle East origin), functional involvement of specific genes, thus resulting in the identification of a homozygous *YME1L1* gene mutation (chr10p12.1).[39] We confirmed the absence of homozygous deleterious variants (missense, nonsense, frameshift, splice site change) in *YME1L1* in the NHLBI Exome Sequencing Project (ESP, http://evs.gs.washington.edu/EVS/; ExAC 0.3 http://exac.broadinstitute.org/), the 1000 Genome database (http://www.1000genomes.org/), the dbSNP138 (http://www.ncbi.nlm.nih.gov/SNP/), and our in-house 898 Middle East origin exome database. The raw data is available under the sequence reads archive (SDA) accession no. SRP073309.

Sanger sequencing of the *YME1L1* gene (NM_014263, GRCh 38.5) confirmed the mutation in

the patients and established the genotype in the other family members and in additional families.

Mouse and human fibroblasts. HAF were established from skin biopsies derived from patient II.5 and unrelated controls (Co1-3). MEF and adult cardiac fibroblasts (ACF) were derived from *Yme1l1* mutant mice (*Yme1l1*$^{loxP/loxP}$) as described previously.[14, 25, 40] HAF, MEF, and ACF were cultured in high glucose Dulbecco's modified Eagle's medium (Gibco, Darmstadt, Germany) supplemented with 15%, 10%, and 10% fetal bovine serum (FBS, Biochrome, Berlin, Germany; Life Technologies; Carlsbad, California), respectively, and 1% penicillin-streptomycin (Sigma Aldrich; St. Louis, Missouri). Fibroblasts were immortalized by stable expression of hTERT and E7.[41]

Generation of *YME1L1*$^{-/-}$ HeLa cells. *YME1L1* KO cells were generated using the CRISPR/Cas9 system. Guide RNA (gRNA) and Cas9 were expressed using the px330 expression vector (Cong et al., 2013). The following gRNA target sequence was used: 5'-GGAACCGACCATATTACAACAGG-3´ (recommended by the lab of Alexander van der Bliek). Single clones were obtained by serial dilution after transfection and screened by SDS-PAGE and immunoblotting.

qPCR. DNA extraction and cDNA synthesis were performed with established methods reported previously.[42] To specifically amplify and detect murine *Yme1l1*, human *YME1L1, Hprt* (Hypoxanthine-guanine phosphoribosyl-transferase, reference gene), and *RPII* (RNA polymerase II, reference gene) cDNA, we designed sets of primers and TaqMan probes specified in **Supplementary file 1A** using the GenScript real-time PCR (TaqMan) Primer Design online software (www.genscript.com). qPCR and quantification was performed as described previously

[42], and further statistics were performed using the GraphPad Prism 5 Software (GraphPad Software Inc., La Jolla, California).

Western blot. Protein whole lysate extraction, fractionated mitochondrial and cytosolic protein extraction, and Western blots were performed with established methods reported previously.[42, 11] Antibodies are listed in **Supplementary file 1B**.

Isolation of a crude mitochondrial fraction.

The protocol was adapted from.[43] Cells were harvested using trypsin and washed three times in PBS to remove the trypsin. Subsequently, the cells were resuspended in 3 ml isotonic Buffer (0,25 M Sucrose, 5 mM Tris-HCL pH 7,5, 1 mM EDTA and 0,1 mM PMSF). The cells were opened with eight strokes by 2500 rpm using a potter homogenisator. Unbroken cells and nuclei were removed by centrifugation at 600x g for 15 minutes at 4 °C. The supernatant was applied to another centrifugation step at 10000x g for 25 minutes at 4 °C. The supernatant contains the cytoplasmic fraction (C) whereas mitochondria are enriched in the pellet. The mitochondrial fraction (M) were washed two times in isotonic buffer and afterwards applied to SDS Page.

Cell viability, apoptosis, and proliferation. Viability and proliferation of HAF were quantified using the Fluorimetric CellTiter-Blue® Cell Viability Assay (Promega, Madison, Wisconsin) and the colorimetric Cell Proliferation BrdU-ELISA (Roche Diagnostics, Rotkreuz, Switzerland), respectively, according to the manufacturer´s instructions. Apoptosis of HAF following treatment with staurosporine (Cell signaling, Cambridge, United Kingdom) was determined through quantification of cleaved PARP protein levels on Western blots.

Mitochondrial respiratory chain enzyme activity. Mitochondrial respiratory chain enzyme activities were measured in skin fibroblasts according to established procedures.[44, 45] The values were expressed relative to the activity of Cytochrome C oxidase and/or Citrate synthase.

Overexpression of human *YME1L1*. Human wild type *YME1L1* and mutant *YME1L1*^{R149W} were stably expressed in Flp-In T-Rex HEK293T cells (Life technologies) under the control of a tetracycline-regulated promotor according to manufacturer´s instructions. HEK293T cells were cultured as described previously.[11] Transient transfection was performed using GeneJuice (EMD Millipore) according to manufacturer´s instruction.

Sucrose gradient density centrifugation. Cells were harvested and washed three times in PBS. Subsequently, the cells were resuspended in isotonic buffer (0,25 M Sucrose, 5 mM Tris-HCL pH 7,5, 1 mM EDTA and 1X cOmplete™, EDTA-free Protease Inhibitor Cocktail (Sigma)). The cells were opened with 15 strokes by 1000 rpm using a Potter S homogenisator (Sartorius). Unbroken cells and nuclei were removed by centrifugation at 600x g for 5 minutes at 4 °C. The supernatant was applied to another centrifugation step at 10000x g for 10 minutes at 4 °C. The mitochondrial-enriched membrane fraction (pellet) was re-suspended in lysis buffer (270 mM sucrose, 100 mM KCl, 20 mM 20 mM $MgCl_2$, 10 mM Tris/HCl, pH 7.5, and 1X cOmplete™, EDTA-free Protease Inhibitor Cocktail) containing 6 g of digitonin per g of protein at a concentration of 2.5 mg/ml for 20 minutes on ice. Supernatant from a clarifying centrifugation at 16,000 g for 10 minutes at 4°C was directly applied to a 5-25% sucrose gradient prepared using an automated gradient maker (Biocomp) in 14x89mm Ultra-Clear centrifuge tubes (Beckman Instruments). Ultracentrifugation was performed at 71,000 x g for 16 h at 4°C and 1.2 ml fractions (n=10) were collected by hand, precipitated by TCA and subjected to SDS-PAGE.

Cell-free synthesis of YME1L1 and processing by purified MPP *in vitro*. The cell-free synthesis of ^{35}S-labeled precursor proteins of human wild type and mutant YME1L1 was performed using the TNT Sp6 or Coupled Reticulocyte lysate system (Promega) according to the manufacturer's instructions. Radiolabeled wild type and mutant YME1L1 were incubated in cleavage buffer (20 mM HEPES, pH 7,4, 50 mM $NaCl_2$, 1 mM Zn Cl_2, 1 mM ATP, 5 mM Mg Cl_2) at 30 °C in the presence of absence of MPP as described previously.[46] Samples were analyzed by SDS-PAGE and autoradiography.

Immunocytochemistry. Immunocytochemistry was performed as described previously.[14, 42] Antibodies are listed in **Supplementary file 1B**; DAPI was purchased from Sigma-Aldrich.

Mitochondrial network analysis. HAF, MEF, and ACF were stained with anti-TOMM20 antibody and DAPI (4′,6-Diamidin-2-phenylindol). Images were taken as described below and quantified in double-blind fashion into four categories: hyperfused, tubular, short tubules and fragmented mitochondrial network as previously described.[14] For the complementation experiments: co-transfection of 100 ng of mitochondrially-targeted GFP (mito-GFP) along with 1 µg of either YME1L1 or YME1L1^{R149W} was performed, and GFP-positive fixed cells were scored for mitochondrial morphology.

Imaging. Fluorescently labeled fibroblasts were imaged with a fluorescent Olympus BX51 microscope using the software Magnafire 2.1B Version 2001 (Olympus, Tokyo, Japan) and a Spinning Disc Microscopy system (Carl Zeiss Microscopy, Oberkochen, Germany) with the ZEN 2012 Software, with an lsm5exciter Zeiss confocal microscope (Carl Zeiss Microscopy). Analysis of overexpression experiment of human wildtype and mutant *YME1L1* was realized with an

358 UltraVIEW VoX spinning disc Yokogawa CSU-X1 confocal microscope (PerkinElmer,
359 Waltham, Massachusetts) on a Nikon Ti microscope equipped with a 60x (Apo TIRF 60x Oil
360 N.A. 1.49) objective and camera (EMCCD C9100-50 CamLink). Imaging of HeLa cells was
361 performed using a Meta 510 confocal laser scanning microscope (Zeiss). All images were
362 processed using Adobe Photoshop (Adobe Systems Inc., San José, California), Volocity
363 (PerkinElmer), and ImageJ (National Institute of Health, USA).
364
365 **Live-cell Imaging.** HAF were cultured on 35 mm Fluorodish Cell Culture Dishes (World
366 Precision Instruments, Sarasota, Florida) and incubated in pre-warmed medium containing 500
367 nM MitoTracker Green® (Thermo Fisher Scientific, Waltham, Massachusetts) 30 min prior to
368 imaging. Live-cell imaging was performed in fresh medium in the microscope incubation
369 chamber (5% CO_2, 37 °C) of a Zeiss Axio Observer with Spinning Disc Technology Carl Zeiss
370 Microscopy) for 7-10 min. Recordings were processed using Adobe Photoshop (Adobe Systems
371 Inc.) and Magix Video Maker Deluxe (Magix Software GmbH, Berlin, Germany).
372
373 **Electron microscopy (EM).** Fibroblasts and muscle biopsy specimen were prepared for TEM
374 analysis and imaged as described previously.[14, 47, 48]
375
376 **Statistical methods.** All results are presented as mean ± SD, GraphPad Prism 5 software was
377 used for all statistical analyses, and the significance level was set at $p<0.05$. Differences between
378 two groups were evaluated by un-paired or paired Student's t-test, while for multi-group
379 comparisons, one-way ANOVA with Tukey's multiple-comparisons test was used. For the
380 mitochondrial fragmentation analysis (Figure 3D), two-way ANOVA followed by the Tukey's
381 multiple-comparisons test was used. Samples sizes, replicate numbers, and p-values are stated in

the figure legends. Replicates are biological replicates except for experiments illustrated in Figures 1H and 2B.

386 **Acknowledgements**

387 The authors thank the family members who participated in this study. We acknowledge T.
388 Burmester for sending us fibroblasts of the affected children, E. Morava-Kozicz, D. Emmerich
389 for sending DNA samples of patients with YME1L1 mitochondriopathy-like phenotypes, as well
390 as G. Stoltenburg-Didinger, V. Tarabykin, C. Birchmeier, N. Krämer, K. Voigt, and J.
391 Fassbender for technical help and discussions. This work was supported by the German Research
392 Foundation (SFB665, KO2891/1-1, Reinhart Koselleck grant), the Berlin Institute of Health
393 (BIH, CRG1), the Sonnenfeld Stiftung, the German Society for Muscle diseases (DGM), the
394 German Academic Exchange Service (DAAD), the NCRR P20-RR016453, the Robert C. Perry
395 Fund (20061479), the Max-Planck Society, the EU FP 7 project GENCODYS (241995), and the
396 Human Frontiers Science Program.

397

398 **Author contributions**

399 CH and AMK recruited subjects, gathered patient history as well as clinical information and
400 contributed clinical samples. WS analyzed patient muscle specimen. HH, LM, HHR, and TFW
401 generated and analyzed WES and performed further mutation analyses in the cohort. BH, TW,
402 TMV and BFZ performed functional experiments. RG helped with imaging. LVDH performed
403 mitochondrial enzyme studies and related DNA studies. AMK, BH, TW and TL drafted the
404 manuscript which was revised and accepted by all coauthors.

405

406 **Competing interests**

407 The authors declare no conflict of interest in the preparation or publication of the data in this
408 manuscript.

References

1. Nunnari J, Suomalainen A. Mitochondria: in sickness and in health. Cell 2012;148:1145-1159.10.1016/j.cell.2012.02.035
2. Campbell CL, Tanaka N, White KH, Thorsness PE. Mitochondrial morphological and functional defects in yeast caused by yme1 are suppressed by mutation of a 26S protease subunit homologue. Mol Biol Cell 1994;5:899-905
3. Thorsness PE, White KH, Fox TD. Inactivation of YME1, a member of the ftsH-SEC18-PAS1-CDC48 family of putative ATPase-encoding genes, causes increased escape of DNA from mitochondria in Saccharomyces cerevisiae. Mol Cell Biol 1993;13:5418-5426
4. Nakai T, Yasuhara T, Fujiki Y, Ohashi A. Multiple genes, including a member of the AAA family, are essential for degradation of unassembled subunit 2 of cytochrome c oxidase in yeast mitochondria. Mol Cell Biol 1995;15:4441-4452
5. Pearce DA, Sherman F. Degradation of cytochrome oxidase subunits in mutants of yeast lacking cytochrome c and suppression of the degradation by mutation of yme1. J Biol Chem 1995;270:20879-20882
6. Leonhard K, Herrmann JM, Stuart RA, Mannhaupt G, Neupert W, Langer T. AAA proteases with catalytic sites on opposite membrane surfaces comprise a proteolytic system for the ATP-dependent degradation of inner membrane proteins in mitochondria. EMBO J 1996;15:4218-4229
7. Shah ZH, Hakkaart GA, Arku B, et al. The human homologue of the yeast mitochondrial AAA metalloprotease Yme1p complements a yeast yme1 disruptant. FEBS Lett 2000;478:267-270
8. Weber ER, Hanekamp T, Thorsness PE. Biochemical and functional analysis of the YME1 gene product, an ATP and zinc-dependent mitochondrial protease from S. cerevisiae. Mol Biol Cell 1996;7:307-317
9. Rainey RN, Glavin JD, Chen HW, French SW, Teitell MA, Koehler CM. A new function in translocation for the mitochondrial i-AAA protease Yme1: import of polynucleotide phosphorylase into the intermembrane space. Mol Cell Biol 2006;26:8488-8497.10.1128/MCB.01006-06
10. Van Dyck L, Langer T. ATP-dependent proteases controlling mitochondrial function in the yeast Saccharomyces cerevisiae. Cell Mol Life Sci 1999;56:825-842
11. Potting C, Tatsuta T, Konig T, et al. TRIAP1/PRELI complexes prevent apoptosis by mediating intramitochondrial transport of phosphatidic acid. Cell Metab 2013;18:287-295.10.1016/j.cmet.2013.07.008
12. Baker MJ, Mooga VP, Guiard B, Langer T, Ryan MT, Stojanovski D. Impaired folding of the mitochondrial small TIM chaperones induces clearance by the i-AAA protease. J Mol Biol 2012;424:227-239.10.1016/j.jmb.2012.09.019
13. Rainbolt TK, Saunders JM, Wiseman RL. YME1L degradation reduces mitochondrial proteolytic capacity during oxidative stress. EMBO Rep 2015;16:97-106.10.15252/embr.201438976
14. Anand R, Wai T, Baker MJ, et al. The i-AAA protease YME1L and OMA1 cleave OPA1 to balance mitochondrial fusion and fission. J Cell Biol 2014;204:919-929.10.1083/jcb.201308006
15. van der Bliek AM, Koehler CM. A mitochondrial rhomboid protease. Dev Cell 2003;4:769-770

16. Delettre C, Lenaers G, Griffoin JM, et al. Nuclear gene OPA1, encoding a mitochondrial dynamin-related protein, is mutated in dominant optic atrophy. Nat Genet 2000;26:207-210.10.1038/79936
17. Cipolat S, Martins de Brito O, Dal Zilio B, Scorrano L. OPA1 requires mitofusin 1 to promote mitochondrial fusion. Proc Natl Acad Sci U S A 2004;101:15927-15932.10.1073/pnas.0407043101
18. Frezza C, Cipolat S, Martins de Brito O, et al. OPA1 controls apoptotic cristae remodeling independently from mitochondrial fusion. Cell 2006;126:177-189
19. Olichon A, Baricault L, Gas N, et al. Loss of OPA1 perturbates the mitochondrial inner membrane structure and integrity, leading to cytochrome c release and apoptosis. J Biol Chem 2003;278:7743-7746.10.1074/jbc.C200677200
20. MacVicar T, Langer T. OPA1 processing in cell death and disease - the long and short of it. J Cell Sci 2016;129:2297-2306.10.1242/jcs.159186
21. Ehses S, Raschke I, Mancuso G, et al. Regulation of OPA1 processing and mitochondrial fusion by m-AAA protease isoenzymes and OMA1. J Cell Biol 2009;187:1023-1036.10.1083/jcb.200906084
22. Griparic L, Kanazawa T, Van Der Bliek AM. Regulation of the mitochondrial dynamin-like protein Opa1 by proteolytic cleavage. J Cell Biol 2007;178:757-764.10.1083/jcb.200704112
23. Head B, Griparic L, Amiri M, Gandre-Babbe S, van der Bliek AM. Inducible proteolytic inactivation of OPA1 mediated by the OMA1 protease in mammalian cells. J Cell Biol 2009;187:959-966.10.1083/jcb.200906083
24. Song Z, Chen H, Fiket M, Alexander C, Chan DC. OPA1 processing controls mitochondrial fusion and is regulated by mRNA splicing, membrane potential, and Yme1L. J Cell Biol 2007;178:749-755.10.1083/jcb.200704110
25. Wai T, Garcia-Prieto J, Baker MJ, et al. Imbalanced OPA1 processing and mitochondrial fragmentation cause heart failure in mice. Science 2015;350:aad0116.10.1126/science.aad0116
26. Coenen MJ, Smeitink JA, Smeets R, Trijbels FJ, van den Heuvel LP. Mutation detection in four candidate genes (OXA1L, MRS2L, YME1L and MIPEP) for combined deficiencies in the oxidative phosphorylation system. J Inherit Metab Dis 2005;28:1091-1097.10.1007/s10545-005-4483-y
27. De Michele G, De Fusco M, Cavalcanti F, et al. A new locus for autosomal recessive hereditary spastic paraplegia maps to chromosome 16q24.3. Am J Hum Genet 1998;63:135-139.10.1086/301930
28. Hazan J, Fontaine B, Bruyn RP, et al. Linkage of a new locus for autosomal dominant familial spastic paraplegia to chromosome 2p. Hum Mol Genet 1994;3:1569-1573
29. Warnecke T, Duning T, Schwan A, Lohmann H, Epplen JT, Young P. A novel form of autosomal recessive hereditary spastic paraplegia caused by a new SPG7 mutation. Neurology 2007;69:368-375.10.1212/01.wnl.0000266667.91074.fe
30. Graef M, Seewald G, Langer T. Substrate recognition by AAA+ ATPases: distinct substrate binding modes in ATP-dependent protease Yme1 of the mitochondrial intermembrane space. Mol Cell Biol 2007;27:2476-2485.10.1128/MCB.01721-06
31. Stiburek L, Cesnekova J, Kostkova O, et al. YME1L controls the accumulation of respiratory chain subunits and is required for apoptotic resistance, cristae morphogenesis, and cell proliferation. Mol Biol Cell 2012;23:1010-1023.10.1091/mbc.E11-08-0674
32. Claros MG, Vincens P. Computational method to predict mitochondrially imported proteins and their targeting sequences. Eur J Biochem 1996;241:779-786

33. Niidome T, Kitada S, Shimokata K, Ogishima T, Ito A. Arginine residues in the extension peptide are required for cleavage of a precursor by mitochondrial processing peptidase. Demonstration using synthetic peptide as a substrate. J Biol Chem 1994;269:24719-24722
34. Rainbolt TK, Lebeau J, Puchades C, Wiseman RL. Reciprocal Degradation of YME1L and OMA1 Adapts Mitochondrial Proteolytic Activity during Stress. Cell Rep 2016;14:2041-2049.10.1016/j.celrep.2016.02.011
35. Baker MJ, Lampe PA, Stojanovski D, et al. Stress-induced OMA1 activation and autocatalytic turnover regulate OPA1-dependent mitochondrial dynamics. EMBO J 2014;33:578-593.10.1002/embj.201386474
36. Korwitz A, Merkwirth C, Richter-Dennerlein R, et al. Loss of OMA1 delays neurodegeneration by preventing stress-induced OPA1 processing in mitochondria. J Cell Biol 2016;212:157-166.10.1083/jcb.201507022
37. Burte F, Carelli V, Chinnery PF, Yu-Wai-Man P. Disturbed mitochondrial dynamics and neurodegenerative disorders. Nat Rev Neurol 2015;11:11-24.10.1038/nrneurol.2014.228
38. Nielsen JE, Koefoed P, Abell K, et al. CAG repeat expansion in autosomal dominant pure spastic paraplegia linked to chromosome 2p21-p24. Hum Mol Genet 1997;6:1811-1816
39. Najmabadi H, Hu H, Garshasbi M, et al. Deep sequencing reveals 50 novel genes for recessive cognitive disorders. Nature 2011;478:57-63.10.1038/nature10423
40. Yao J, Shoubridge EA. Expression and functional analysis of SURF1 in Leigh syndrome patients with cytochrome c oxidase deficiency. Hum Mol Genet 1999;8:2541-2549
41. Zhu Z, Yao J, Johns T, et al. SURF1, encoding a factor involved in the biogenesis of cytochrome c oxidase, is mutated in Leigh syndrome. Nat Genet 1998;20:337-343.10.1038/3804
42. Issa L, Kraemer N, Rickert CH, et al. CDK5RAP2 expression during murine and human brain development correlates with pathology in primary autosomal recessive microcephaly. Cereb Cortex 2013;23:2245-2260.10.1093/cercor/bhs212
43. Vogel RO, Janssen RJ, Ugalde C, et al. Human mitochondrial complex I assembly is mediated by NDUFAF1. FEBS J 2005;272:5317-5326.10.1111/j.1742-4658.2005.04928.x
44. Janssen AJ, Trijbels FJ, Sengers RC, et al. Measurement of the energy-generating capacity of human muscle mitochondria: diagnostic procedure and application to human pathology. Clin Chem 2006;52:860-871.10.1373/clinchem.2005.062414
45. Smeitink J, Sengers R, Trijbels F, van den Heuvel L. Human NADH:ubiquinone oxidoreductase. J Bioenerg Biomembr 2001;33:259-266
46. Nolden M, Ehses S, Koppen M, Bernacchia A, Rugarli EI, Langer T. The m-AAA protease defective in hereditary spastic paraplegia controls ribosome assembly in mitochondria. Cell 2005;123:277-289.10.1016/j.cell.2005.08.003
47. Stenzel W, Preusse C, Allenbach Y, et al. Nuclear actin aggregation is a hallmark of anti-synthetase syndrome-induced dysimmune myopathy. Neurology 2015;84:1346-1354.10.1212/WNL.0000000000001422
48. Wakabayashi J, Zhang Z, Wakabayashi N, et al. The dynamin-related GTPase Drp1 is required for embryonic and brain development in mice. J Cell Biol 2009;186:805-816.10.1083/jcb.200903065

Figures and Tables

Figure 1. Phenotype and genotype of patients with YME1L1 mitochondriopathy. (**A, B**) The four affected patients are children of healthy, consanguineous parents of Saudi Arabian decent (□ male; ○ female; ◇ unknown gender; ∅/⊠ deceased; ◧/◐ heterozygous, clinically not affected; ●/■ homozygous, affected; ═, consanguineous marriage). (**C**) Cranial MRIs reveal hyperintense changes (arrows) as a sign for leucencephalopathy, and cerebral atrophy (FLAIR, axial images). (**D**) Histological analysis of patient II.5 muscle biopsy specimen, from left to right: Gomori trichrome stain for muscle fibers revealed no conspicuous ragged red fibers indicative of a mitochondriopathy. Succinate dehydrogenase (SDH) and neuron specific enolase (NSE) staining revealed a neurogenic pattern with grouped fibers indicating denervation (magnification 200x). Electron microscopy (EM) revealed paracristalline inclusions (arrow) and altered cristae structure ("parking lots", magnification 15,000x). (**E**) Whole exome sequencing discovered the homozygous mutation c.616C>T in exon 5 of the *YME1L1* gene (NM_014263), localized at position 149 of the YME1L1 protein, and leading to an amino acid exchange of arginine to tryptophan in the mitochondrial targeting site (MTS; p.R149W, NP_055078). YME1L1 contains highly conserved domains: MTS, transmembrane domain (TM), ATPase domain (AAA+), motif of metalloprotease (Zinc) activity (HESGH). (**F**) Electropherogram depicting homozygous missense mutation in patient II.5, which is heterozygous in the father. (**G**) The mutation lies within a protein region, highly conserved throughout different species. (**H**) YME1L1 mRNA levels do not differ between patient and control HAF (n=6; ns, not significant; p=0.2314; one-way ANOVA, HAF, primary human adult fibroblasts) (**I**) Steady state levels of YME1L1 are below detection levels or profoundly reduced in cell lysates of patient II.5 YME1L1^{R149W}; *Yme1l1* knockout mouse fibroblasts serve as negative controls. YME1L1 protein levels in mitchondrial compartment fractions can be found Figure 1I-Figure Supplemental (ACF,

566 immortalized murine adult cardiac fibroblasts; MEF, immortalized murine embryonic fibroblast;
567 WT, wild type; KO, *Yme1l1* knockout, n=5).
568
569 **Figure 2. Mutation of arginine 149 impairs maturation of YME1L1 by MPP upon import**
570 **into mitochondria. (A)** YME1L1^{R149W} is targeted to mitochondria. HeLa cells were transiently
571 transfected with wild-type YME1L1, YME1L1^{R149W} or the empty vector (EV) as control. Cells
572 were analyzed by indirect immunofluorescence and co-localization of the immunofluorescent
573 signals of antibodies against YME1L1 and ATP Synthase subunit beta (ATPase-ß) (WT,
574 Wildtype; KO, Knockout; EV, empty vector; YME1L1^{R149W}, patient mutation; Scale bar 10 µM)**.**
575 (**B**) Inhibition of the proteasome with MG132 (20 mM, 18 h) does not stabilize precursor or
576 mature YME1L1 in Flp-In T-Rex HEK293T cells expressing YME1L1 or YME1L1 mutant
577 variants: R149W, E381Q or R149W/E381Q. P4D1 antibodies were used as control for ubiquitin
578 accumulation and proteasome inhibition. (*, unspecific signal; p, premature; m, mature; E381Q,
579 dominant negative mutation of ATPase domain; R149W, patient mutation; R149W/E381Q,
580 double mutant, n=2). (**C**) Maturation of YME1L1 is mediated by MPP and impaired upon
581 mutation of arginine 149. After site-directed mutagenesis of N-terminal arginine residues in
582 YME1L1, the mutant proteins were expressed in a cell-free system and processing by
583 recombinant MPP was examined (WT, wild type YME1L1; YME1L1^{R149W}, patient mutant
584 YME1L1; p, premature m, mature, n=2-3). (**D**) Cell-free MPP cleavage-assay: MPP can cleave
585 YME1L1 but not YME1L1^{R149W} from the premature to its mature form (n=3)
586
587
588

Figure 3. Mutation of arginine 149 destabilizes YME1L1 but retains residual YME1L activity.

(**A**) Stability of YME1L1 or YME1L1 mutant variants (R149W, E381Q and R149W/E381Q) expressed in Flp-In T-Rex HEK293T cells. The dominant negative E381Q mutation in the ATPase domain of YME1L1 prevents degradation of YME1L1^{R149W} (CHX, cycloheximide; p, premature; m, mature; E381Q, dominant negative mutation of ATPase domain; R149W, patient mutation; R149W/E381Q, double mutant; SDHA, succinate dehydrogenase; h, hours; n=2). (**B**) Homozygous mutations in *YME1L1* results in an accumulation of PRELID1 in the human patient. *Yme1l1* knockout mouse fibroblasts serve as positive controls to demonstrate impaired proteolysis of PRELID1 (n=5). (**C**) Mutation of arginine 149 of YME1L1 impairs processing of OPA1 with a decrease of short OPA1 form d levels. The formation of OPA1 form d indicates residual YME1L1 activity in human patient fibroblasts (immort. HAF, immortalized human adult fibroblasts; n=6). The schematic diagram illustrates the proteolytic processing of OPA1 by YME1L1 on processing site 2 (S2) and OMA1 on processing site 1 (S1). Presence of long OPA1 forms (L-OPA1) is required for the maintenance of mitochondrial inner membrane fusion, whereas accumulation of short OPA1 forms (S-OPA1) is associated with accelerated fission. (**D**) Mitochondria-enriched membrane fractions from Flp-In T-Rex HEK293T cells expressing YME1L1 or YME1L1 mutant variants (R149W, E381Q and R149W/E381Q) were solubilized in digitonin and analyzed by sucrose gradient centrifugation. Fractions were collected and separated on SDS-PAGE for immunoblotting to detect high MW complexes of YME1L1. HSP60 complexes were used as a control (M, mitochondrial input, P, S, pellet and supernatant fraction after solubilization; HSP60, heat shock protein 60; E381Q, dominant negative mutation of ATPase domain; R149W, patient mutation; R149W/E381Q, double mutant). (**E**) Premature YME1L1/ YME1L1^{R149W} is imported into the mitochondrial matrix via translocons of the outer

mitochondrial membrane (TOMM) and inner mitochondrial membrane (TIMM). Here, MPP binds and cleaves the N-terminal mitochondrial targeting site (MTS) from premature YME1L1 but not YME1L1^{R149W}, which then allows the mature and premature YME1L1^{R149W} protein to assemble as proteolytic complex.

Figure 4. YME1L1^{R149W} causes mitochondrial fragmentation. (**A, B**) YME1L1^{R149W} causes fragmentation (fragmentation or short tubules) of mitochondrial networks in patient fibroblasts (n=150-200 cells, 4 replicates, one-way ANOVA, scale bar 10 µm). (**C**) Co-transfection of mitochondrial GFP and human YME1L1/ YME1L1^{R149W} protein in WT and *Yme1l1*$^{(-/-)}$ MEFs revealed that YME1L1 but not YME1L1^{R149W} can rescue mitochondrial fragmentation in *Yme1l1*$^{(-/-)}$ MEFs and (**D**) increases the number of cells with tubular networks. Expression of YME1L1^{R149W} partially rescues the fragmentation phenotype. In WT MEFs, YME1L1^{R149W} expression results in only a mild, but not significant decline of cells with a tubular mitochondrial network (two-way ANOVA; n=3; scale bar 10 µm; **p<0.01; ***p<0.001; ****p<0.0001).

Figure 5. YME1L1 mutation impairs fibroblast cell growth and proliferation. (**A**) Significant reduction of cell culture growth and (**B**) proliferation of patient HAF after 120h under culture conditions (n=5; one-way ANOVA; *** p<0.001; ****p<0.0001). (**C**) No increase in apoptosis-sensitivity upon 2 µM staurosporine (STS) treatment in patient HAF after 6h (SDS-PAGE for cleaved PARP level (cPARP) (n=3; one-way ANOVA; p6h = 0.4283). (**D**) Normal respiratory chain subunit activity in patient HAF (U, units; mU, milli U; CS, Citrate synthase). (**E**) Cytochrome c oxidase subunit 4 (COX4) and NADH ubiquinone oxidoreductase 1 beta subcomplex 6 (NDUFB6) protein levels were not elevated in patient fibroblasts (n=3). (**F**) Decreased levels of mitochondrial compartment markers TOMM20 (translocon of outer

637 mitochondrial membrane 20) for the outer membrane (OM), Cytochrome c for the intermembrane
638 space (IMS), SDHA (succinate dehydrogenase) for the inner membrane (IM), and Cyclophilin D
639 for the matrix in whole cell lysates of patient II.5 (n=3).
640

641 **Table 1: *YME1L1* mitochondriopathy phenotype.**

Pedigree ID (gender)			II.5 (f)	II.8 (f)	II.9 (m)	II.11 (f)
Age at last assessment (y)			15.8	12.3	10.3	5.2
Category	**Feature**	**HPO**				
Inheritance						
			AR	AR	AR	AR
Growth						
Height	Short stature SD; %	0004322	+ -2.19; 1	+ -2.09; 2	+ -1.89; 3	- 0.38; 35
Weight	Low weight SD; %	0004325	+ -2.8; <1	- -1.18; 12	- 0.07; 53	- -1.35; 12
Neonatal period						
	Neonatal asphyxia	0012768	-	-	-	+
Head and Neck						
Head	Microcephaly	0000252	-	-	+	+
	Macrocephaly	0000256	+	-	-	-
Face	Midface retrusion	0011800	-	-	+	+
	Congenital facial diplegia	0007188	+	-	-	+
Ears	Hearing impairment	0000365	-	+	+	+
	Sensorineural hearing impairment	0000407	n.a.	n.a.	+	+
	Macrotia	0000400	-	+	+	-
Eyes	Pigmentary retinopathy	0000580	+	-	-	-
	Optic nerve hypoplasia	0000609	+	+	+	+
	Cherry red spot of the macula	0010729	-	-	-	+
	Strabismus	0000486	-	-	+	+
	Hypermetropia	0000540	-	-	-	+
	Myopia	0000545	+	+	+	-
	Amblyopia	0000646	-	+	+	+
	Abnormality of visual evoked potentials	0000649	n.a.	-	+	+
Abdomen						
Gastro-intestinal	Constipation (in infancy)	0002019	+	n.a.	+	+
Spleen	Splenomegaly	0001744	+	-	+	-
Skeletal						
Feet	Bilateral talipes equinovarus	0001776	-	-	-	+
Muscle, soft tissue						
	Increased variability in muscle fiber diameter	0003557	+	n.a.	n.a.	n.a.
Neurologic						

CNS	Hypotonia, neonatal, generalized	0008935	-	-	-	+
	Infantile muscular hypotonia	0008947	-	-	-	+
	Global developmental delay (onset, months)	0001263	+	+	+	+ (6)
	Motor delay	0001270	+	+	+	+
	Gait apraxia	0010521	-	-	-	+
	Athetosis	0002305	-	-	-	+
	Intellectual disability, moderate; (IQ)	0002342	+ (48)	n.a.	n.a.	+ (39)
	Incomprehensible speech	0002546	n.a.	-	-	+
	Poor speech	0002465	n.a.	-	+	-
	Absent speech	0001344	-	+	-	-
	Seizures (onset, months)	0001250	-	-	-	+ (6)
	Dysmetria	0001310	+	+	+	-
	Ataxia	0001251	+	+	+	-
	Brain atrophy	0012444	-	-	-	+
	Ventriculomegaly	0002119	-	-	-	+
	Delayed CNS myelination	0002188	+	-	-	-
	Abnormality of the cerebral white matter	0002500	+	+	+	+
	Abnormality of the basal ganglia	0002134	-	-	+	-
	Cerebellar hypoplasia (progressive)	0001321	+	-	-	+
	EEG with focal sharp waves	0011196	n.a.	-	+	-
	Abnormal auditory evoked potentials	0006958	n.a.	n.a.	+	+
PNS	Decreased sensory nerve conduction velocity	0003448	-	+	n.a.	-
Behavioural Psychiatric	Hyperactivity	0000752	-	+	-	-
	Attention deficit hyperactivity disorder	0007018	-	-	-	+
	Stereotypical body rocking	0012172	-	-	-	+
Laboratory anomalies						
	Mildly elevated creatine phosphokinase	0008180	-	-	-	+

642

Abbreviations: AR, autosomal recessive; CNS, central nervous system; PNS, peripheral nervous system; EEG, electroencephalogram; f, female; HPO, human phenotype ontology (http://www.human-phenotype-ontology.org/); m, male; n.a., not assessed; %, percentile; SDS, standard deviation score; y, years)

Supplementary material

Figures

Figure 1I–figure supplement 1: YME1L1^{R149W} signal is barely detectable in total cell lysates (T), significantly reduced in the mitochondrial (M) but not present in the cytosolic (C) fraction of patient HAF (n=3).

Rich media/Videos

Video 1. Three dimensional rendering of mitochondrial structure of a control fibroblast. MitoTracker Deep Red®- mitochondria; DAPI-nucleus.

Video 2. Three dimensional rendering of mitochondrial structure of a patient II.5 fibroblast. MitoTracker Deep Red®- mitochondria; DAPI-nucleus.

Video 3. Mitochondrial dynamics in a control fibroblast. MitoTracker® Green-mitochondria, live cell imaging.

Video 4. Mitochondrial dynamics in a patient II.5 fibroblast. MitoTracker® Green-mitochondria, live cell imaging.

Tables

Supplementary file 1A. List of primers for qPCR and genotyping

Supplementary file 1B. List of primary and secondary antibodies

Source data

Figure 1H–Source data 1.

Raw data Graph 1H. Raw values of YME1L1 mRNA expression in human adult fibroblasts of controls and patient measured via TaqMan qPCR (n=6).

Figure 4B–Source data 1

Raw data Graph 4B. Relative mitochondrial morphology quantification after immunocytochemistry with TOMM20 antibody and DAPI in human adult fibroblasts of control and patient (n=150-200 cells, 4 replicates).

Figure 4D–Source data 1

Raw data Graph 4D. Relative mitochondrial morphology quantification after immunocytochemistry with TOMM20 antibody and DAPI in WT and *Yme1l1*$^{-/-}$ adult cardiac murine fibroblasts overexpressing YME1L1 or YME1L1^{R149W} (n=3).

Figure 5A–Source data 1

Raw data Graph 5A. Raw values of fluorometric measurement with Cell-titer Blue Cell Viability Assay application in human adult fibroblasts of controls and patient (n=5).

Figure 5B–Source data 1

Raw data Graph 5B. Raw values of colorimetric measurement with BrdU Cell Proliferation ELISA Assay application in human adult fibroblasts of controls and patient (n=5).

Figure 5C–Source data 1

Raw data Graph 5C. Raw values of cleaved-PARP antibody signal intensity after staurosporine treatment in human adult fibroblasts of controls and patient and SDS-Page (n=3).

Figure 1

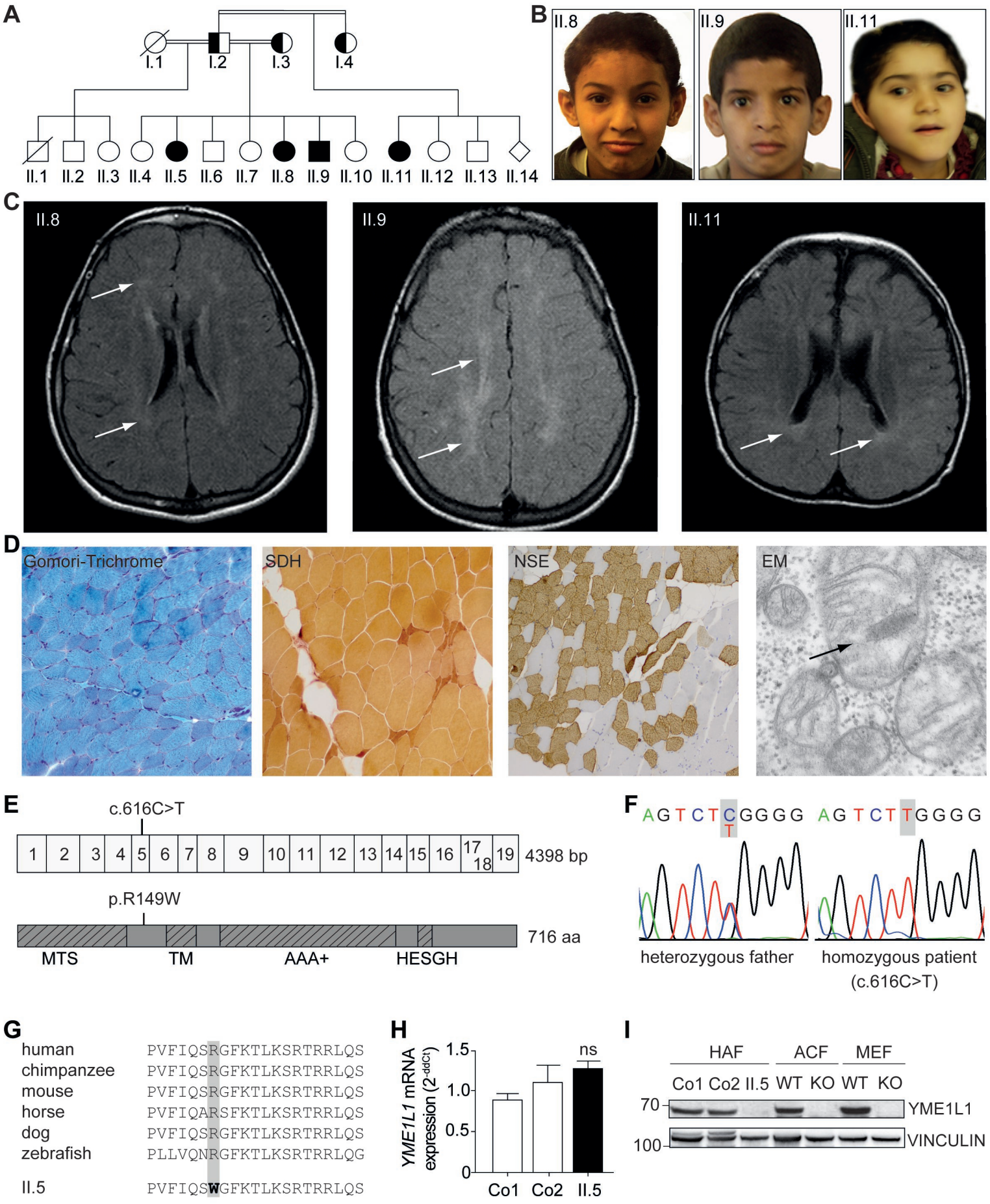
A
I.1
I.2
I.3
I.4
II.1
II.2
II.3
II.4
II.5
II.6
II.7
II.8
II.9
II.10
II.11
II.12
II.13
II.14
B
II.8
II.9
II.11
C
II.8
II.9
II.11
D
Gomori-Trichrome
SDH
NSE
EM
E
c.616C>T
1
2
3
4
5
6
7
8
9
10
11
12
13
14
15
16
17
18
19
4398 bp
p.R149W
716 aa
MTS
TM
AAA+
HESGH
F
AGTCTCGGGG
AGTCTTGGGG
heterozygous father
homozygous patient
(c.616C>T)
G
human PVFIQSRGFKTLKSRTRRLQS
chimpanzee PVFIQSRGFKTLKSRTRRLQS
mouse PVFIQSRGFKTLKSRTRRLQS
horse PVFIQARSFKTLKSRTRRLQS
dog PVFIQSRGFKTLKSRTRRLQS
zebrafish PLLVQNRGFKTLKSRTRRLQG
II.5 PVFIQSWGFKTLKSRTRRLQS
H
YME1L1 mRNA expression (2-ddCt)
1.5
1.0
0.5
0
ns
Co1
Co2
II.5
I
HAF
ACF
MEF
Co1 Co2 II.5 WT KO WT KO
70
YME1L1
100
VINCULIN

Figure 2

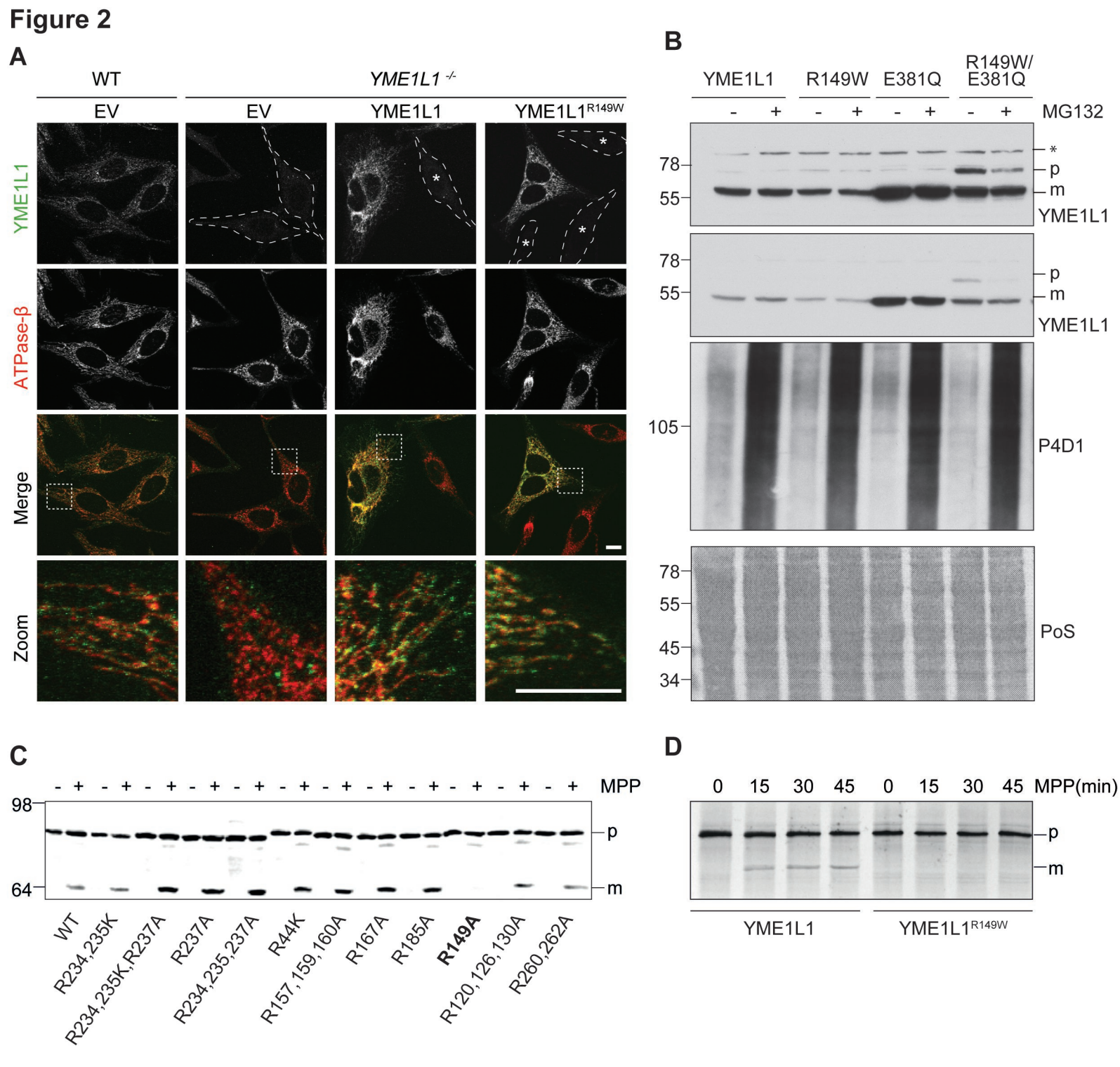
A
WT
YME1L1 -/-
EV
EV
YME1L1
YME1L1R149W
YME1L1
ATPase-β
Merge
Zoom
B
YME1L1
R149W
E381Q
R149W/ E381Q
MG132
78
55
105
45
34
p
m
YME1L1
P4D1
PoS
C
MPP
98
64
WT
R234,235K
R234,235K,R237A
R237A
R234,235,237A
R44K
R157,159,160A
R167A
R185A
R149A
R120,126,130A
R260,262A
D
0 15 30 45 0 15 30 45 MPP(min)
YME1L1
YME1L1R149W

Figure 3

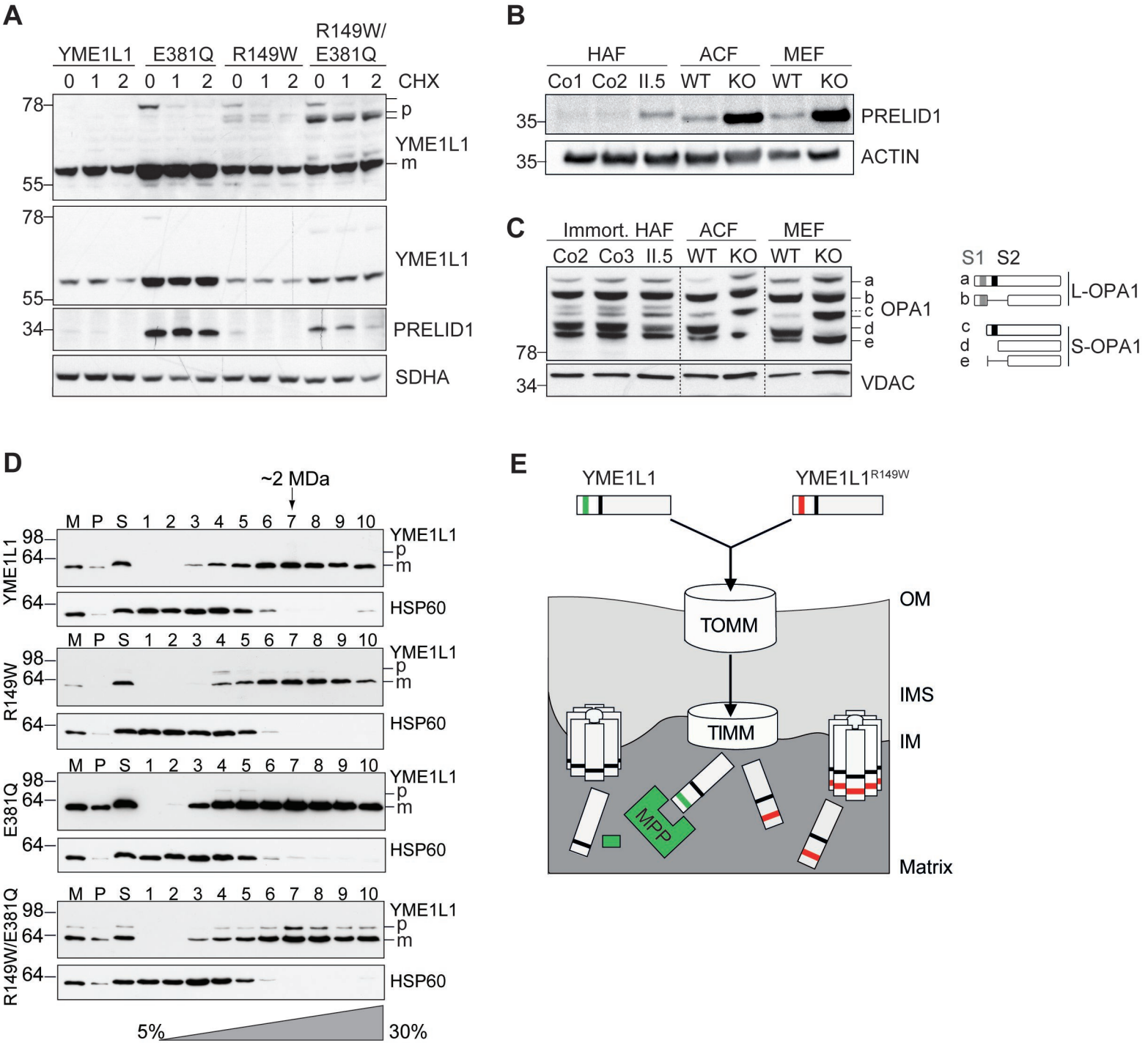
A
YME1L1
E381Q
R149W
R149W/ E381Q
0 1 2 0 1 2 0 1 2 0 1 2 CHX
78
55
p
m
YME1L1
78
55
YME1L1
34
PRELID1
SDHA
B
HAF
ACF
MEF
Co1 Co2 II.5 WT KO WT KO
35
PRELID1
35
ACTIN
C
Immort. HAF
ACF
MEF
Co2 Co3 II.5 WT KO WT KO
a
b
c
d
e
OPA1
78
34
VDAC
S1 S2
L-OPA1
S-OPA1
D
~2 MDa
M P S 1 2 3 4 5 6 7 8 9 10
YME1L1
R149W
E381Q
R149W/E381Q
98
64
YME1L1
p
m
HSP60
5%
30%
E
YME1L1
YME1L1R149W
TOMM
TIMM
MPP
OM
IMS
IM
Matrix

Figure 4

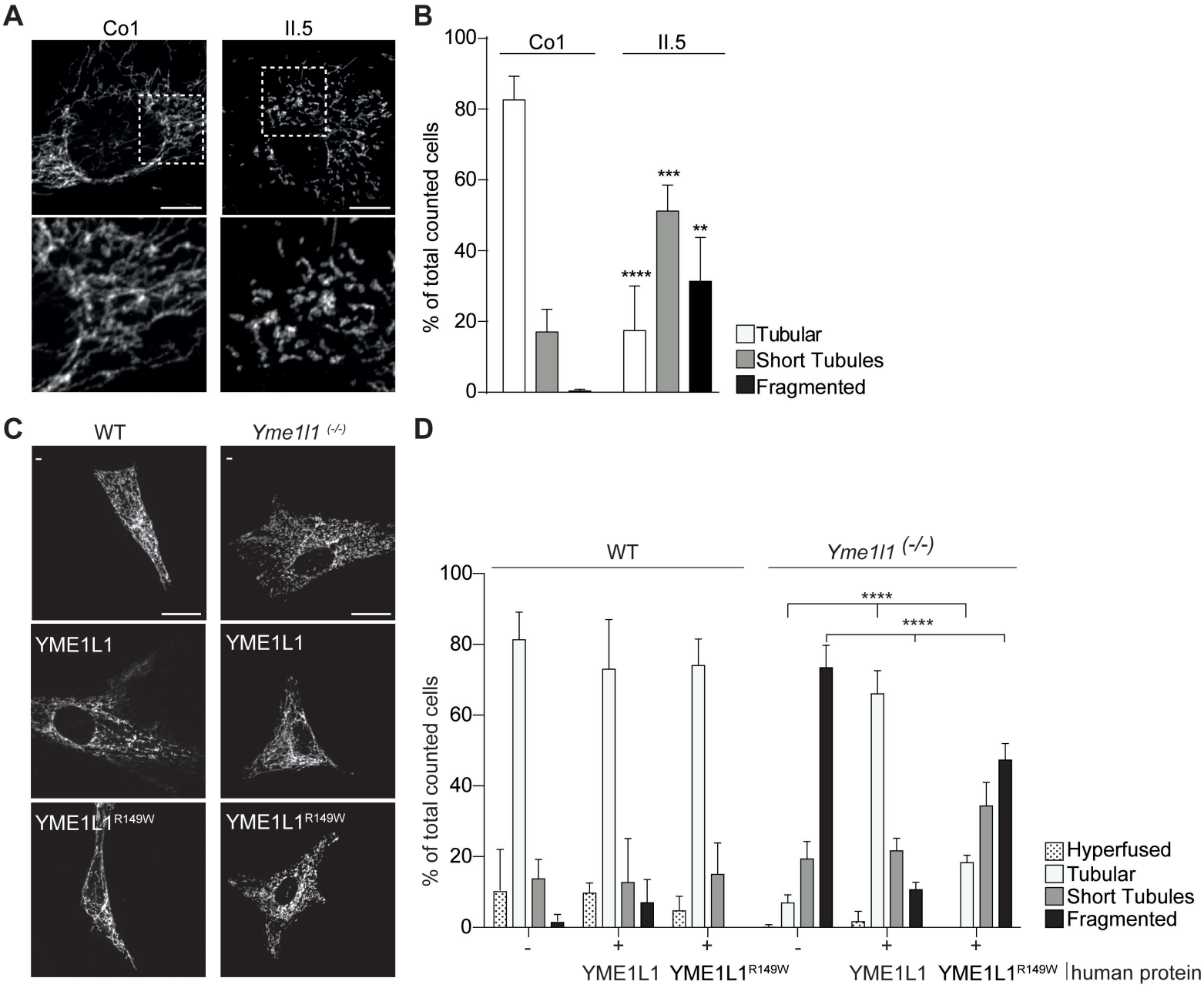
A
Co1
II.5
B
Co1
II.5
% of total counted cells
Tubular
Short Tubules
Fragmented
C
WT
Yme1l1 (-/-)
YME1L1
YME1L1R149W
D
WT
Yme1l1 (-/-)
% of total counted cells
Hyperfused
Tubular
Short Tubules
Fragmented
YME1L1
YME1L1R149W
human protein

Figure 5

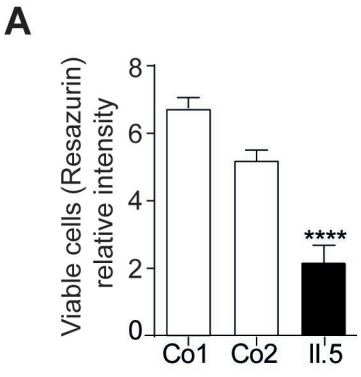

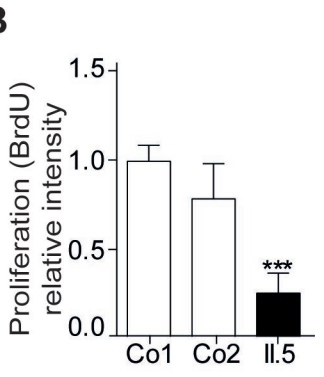

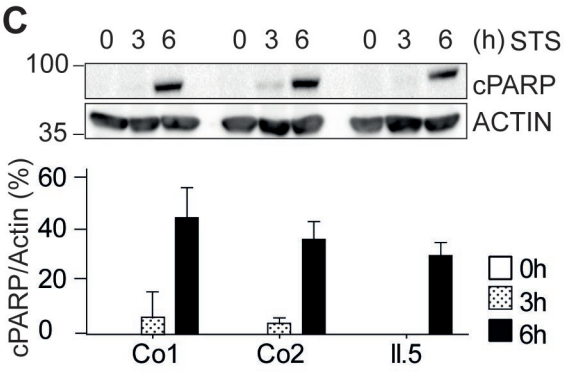

D

Respiratory chain complex	Unit	II.5	Reference activity
Complex I	mU/U CS	411	163 - 599
Complex II	mU/U CS	560	335 - 888
Complex III	mU/U CS	1064	570 - 1383
Complex II+III	mU/U CS	270	128 - 534
Complex IV	mU/U CS	532	288 - 954
Complex V	mU/U CS	773	193 - 819
Citrat Synthase	mU/mg protein	210	151 - 449